Investigation of the instability mechanisms in a turbocharger centrifugal compressor with a vaneless diffuser by means of unsteady simulations

Xinqian Zheng, Anxiong Liu and Zhenzhong Sun

Abstract
The stable-flow range of a compressor is predominantly limited by surge and stall. In this paper, an unsteady simulation method was employed to investigate the instability mechanisms of a high-speed turbocharger centrifugal compressor with a vaneless diffuser. In comparison with the variation in the pressure obtained by dynamic experiments on the same compressor, unsteady simulations show a great accuracy in representing the stall behaviour. The predicted frequency of the rotating stall is 22.5% of the rotor frequency, which agrees with to the value for the high-frequency short-term rotating stall obtained experimentally. By investigating the instability of the flow field, it is found that the unstable flow of the turbocharger compressor at high rotational speeds is caused by the tip clearance leakage flow and the 'backflow vortices' originating from the interaction of the incoming flow and the backflow in the tip region of the passages. The asymmetric volute helps to induce the occurrence of stall in certain impeller passages because it generates an asymmetric flow field. The high-pressure low-velocity area from the 180° circumferential position to the 270° circumferential position is dominant and strengthens the backflow at the trailing edge of the impeller, finally triggering the stall.

Introduction

The internal-combustion engines (ICEs) that are used in automobiles are responsible for a large proportion of fossil fuel energy consumption and emissions, and the potential of ICEs to conserve energy and to reduce emissions is considerable. One of the most influential technologies is engine downsizing through turbocharging.[1] Turbocharging increases the density of the air taken in by the ICE, which increases the power density and allows engines to be downsized significantly, thereby reducing the fuel consumption and the carbon dioxide (CO_2) emissions.[2] Because of the lower heat losses, downsizing also increases the mechanical efficiency and reduces the weight of a vehicle.[2,3] However, the turbocharger compressor has an inherent limitation of aerodynamic stability, which significantly limits the performance of the turbocharger and its ability to provide boost, particularly at low engine speeds.

The stable flow range of a turbocharger and the turbocharged ICE is limited by the aerodynamic

instability of the compressors, which is known as surge and stall. Based on the large numbers of experiments and numerical simulations in compressors and, in particular, in axial compressors, the mechanisms of the instability have been gradually understood. Surge is most often recorded, with audible thumping, honking, pressure oscillations throughout the machine and even reverse mass flow monitored in the inlet.[4] In the 1970s, Greitzer[5–7] developed a one-dimensional non-linear model and a non-dimensional lumped parameter B to predict the instability patterns of the compression

Turbomachinery Laboratory, State Key Laboratory of Automotive Safety and Energy, Tsinghua University, Beijing, People's Republic of China
These authors contributed equally to this work.

Corresponding author:
Xinqian Zheng, Turbomachinery Laboratory, State Key Laboratory of Automotive Safety and Energy, Tsinghua University, Beijing 100084, People's Republic of China.
Email: zhengxq@tsinghua.edu.cn

systems, including deep surge, mild surge and rotating stall. With more experiments[8–12] on rotating stall, Moore[13,14] and Moore et al.[15,16] started to add the geometric parameters of the compressor to their non-linear models, simulating the effect of blades through an actuator disc model and theoretically analysing the two-dimensional modal behaviour. Thereafter, on the basis of the Moore–Greitzer actuator disc model, Bonnaure[17] and Spakovszky et al.[18] solved the Euler equations for specific subcomponents to seek the instability modes in a multi-stage compressor and a centrifugal compressor respectively.

In the 1990s, Day[19–21] discovered a three-dimensional (3D) spike-type stall, which showed an abrupt 'short-length-scale' disturbance appearing as an upward spike in the pressure measurement and circumferentially rotating at 60–80% of the rotor speed, compared with 20–50% for the modal-type stall. The spectacular growth of computational fluid dynamics (CFD) has promoted 3D numerical simulations of compressor stall, and many features of the instability found by dynamic measurements and particle image velocimetry (PIV)[22–24] have been simulated by CFD with some accuracy.[25] Moreover, novel instability mechanisms have been found by unsteady-flow CFD methods.[26,27] Vo[28] and Vo et al.[29] proposed that the net upstream mass flow at the trailing-edge blade tip and the leading-tip clearance below the blade tip are the two criteria for the formation of spike disturbances. Lei et al.[30] claimed that flow reversal occurs on both the blade suction surface and the end wall in axial compressors, which is referred to as a 'hub-corner stall'.

However, few investigations have studied the mechanisms of the aerodynamic instability of the compressor from the perspective of the volute asymmetry. In fact, unlike axial compressors and typical centrifugal compressors in aero-engines or gas turbines, a turbocharger centrifugal compressor includes a volute, which is a circumferentially asymmetric-structure component following the diffuser. The asymmetric volute is usually designed as a spiral-shaped overhung housing that acts as a diffuser at lower flow rates but as a nozzle at higher flow rates than the design values. This situation causes an asymmetric pressure distribution in the diffuser exit, which has a significant impact on the upstream components[31–33] and even on the impeller by reducing the performance, particularly in the stable flow range. Zheng et al.[34] reported numerical estimations of the impact of the asymmetric volute on the stability of a turbocharger centrifugal compressor with a vaneless diffuser and found that the stable flow range was constricted by up to 42% at the design speed, indicating that the volute harms the flow stability severely. Lin et al.[35] conducted experiments based on a unique evaluation method, which showed that the stable flow range was constricted by up to 47% at the design speed because of the volute asymmetry.

For the mechanisms of the aerodynamic instability with regard to the volute asymmetry, Zheng et al.[36,37]

considered the stall inception to be related to the circumferential asymmetric distribution based on the steady simulation results. However, the relationship is not explicit; the way in which the main instability features are affected by the volute asymmetry in the whole flow field of the turbocharger compressor is not known. In this paper, the impeller–diffuser–volute interaction is investigated during the evolution of instability using unsteady 3D CFD supported by dynamic experimental results.

Numerical methodology

The compressor studied is a high-speed small-scale turbocharger centrifugal compressor, which is the same as used in the experiments in the work by Zheng et al.[38,39] It is applied to a four-cylinder diesel engine with a maximum power output of 105 kW, which drives trucks, midi-buses and tourist buses. The main geometric parameters of the compressor are given in Table 1. The fluid domain includes the whole-passage impeller, the vaneless diffuser and the volute housing. Before arriving at the impeller inlet, the incoming flow fully develops through a duct 100 mm long extended in front of the impeller and becomes relatively uniform. The fluid domain is shown in Figure 1.

The 3D Reynolds-averaged Navier–Stokes (RANS) equations for a compressible fluid are solved using the commercial CFD software ANSYS CFX. Large eddy simulations (LESs) have also been used to simulate the features of the instability of the compressor. For instance, a single-blade passage was calculated by Hah et al.[40] The combination of LESs and the RANS method has also been used[41] and, in this method, the wall boundary layer and the separated flow were adopted as an RANS region. However, it is quite computationally expensive to use LESs for a single flow-passage simulation, and very expensive for simulations of the whole annulus. Therefore, the RANS equations remain the mainstream numerical method for the 3D simulations of compressor aerodynamics.

Table 1. Specifications of the centrifugal compressor.

| Parameter	Value or description
Diameter of the impeller tip inlet	44.56 mm
Angle of the impeller tip inlet	−62.5°
Diameter of the impeller tip exit	61.26 mm
Angle of the impeller tip exit	−35°
Height of the impeller exit blade	4 mm
Number of impeller blades	6 main blades, 6 splitter blades
Diffuser type	Vaneless diffuser
Diameter of the diffuser inlet	68.26 mm
Diameter of the diffuser exit	100.00 mm
Width of the diffuser	3.13 mm
Maximum rotational speed	185,000 r/min
Maximum tip speed	593 m/s

Table 2. Mesh data for each component.

Parameter	Value for the following			
	Inlet duct	Impeller	Diffuser	Volute
Number of elements	247,555	4,277,566	615,888	2,671,347
Minimum face angle	33.34°	17.67°	87.93°	—
Maximum length ratio	593.1	2967.6	802.4	—
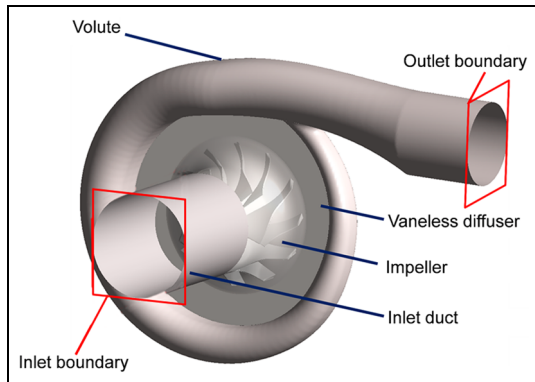
Figure 1. Computational fluid domain.

Figure 2. Mesh created for the whole computational fluid domain.

In this paper, the shear stress transport (SST) turbulence model proposed by Menter[42,43] is used to simulate the unsteady flow. This model takes advantage of the standard Wilcox k–ω model in the near-wall region to predict the severe adverse pressure gradient flows and separation flows, whereas the k–ε model is applied in the main streamline region, which avoids the excess sensitivity to the turbulence parameters and the long computation time necessary if the k–ω model were used. Furthermore, a modification to the turbulent viscosity is introduced into the SST model by the mixed function from the boundary layer to the main flow region; this improves the prediction of turbulent SST, making the SST model more suitable for complex flows, including strong adverse pressure gradient flows and separation flows, which are typical attributes of the unstable aerodynamic flows in the compressor.

The mesh for the whole computational fluid domain is displayed in Figure 2. The structured mesh was developed in ANSYS TurboGrid for the impeller. When the number of elements in each passage is larger than 3.5×10^5, grid independence is satisfied. The structured mesh was also developed for the inlet duct and the diffuser, whereas an unstructured mesh with a prism boundary layer was used for the volute. The mesh data for different components are shown in Table 2.

Y^+ represents the non-dimensional wall distance along the wall and is crucial for accurately representing the phenomena that develop in the boundary layer. Importantly, the reasonable region of Y^+ depends on the numerical method of the solver. The CFX manual suggests $Y^+ < 2$ if the maximum benefits of the SST k–ω model are taken. For the situation in which the
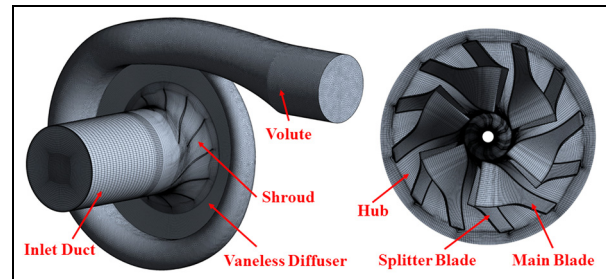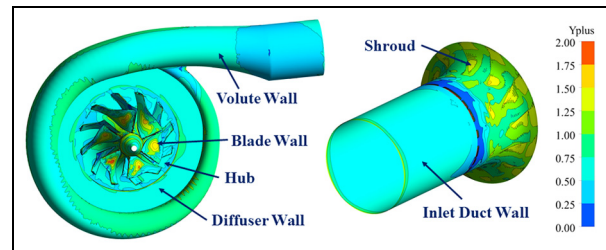
Figure 3. Y^+ distribution in all walls.

height of the first layer of the mesh is controlled, the Y^+ distribution for all walls is shown in Figure 3. It can be seen clearly that Y^+ at all walls is less than 2.0, indicating that the mesh used is suitable for application to the SST turbulence model.

Validation of CFD

Eight specific cross-sections were selected to monitor the unsteady-flow parameters, as shown in Figure 4: the cross-section a of the inlet of the compressor impeller; the leading edge cross-section b of the splitter blade; the cross-section c of the midsection of the impeller; the cross-section d of the inlet of the vaneless diffuser; two cross-sections e and f of the diffuser; the cross-section g of the outlet of the vaneless diffuser; the cross-section h of the volute. The observation points for the impeller are located 0.2 mm from the shroud surface, whereas those for the diffuser are located at the midpoint between the hub and shroud, and those for the volute lie on the centre-line. Each cross-section has six uniformly distributed observation points, located at the positions 0°, 60°, 120°, 180°, 240° and 300° in the
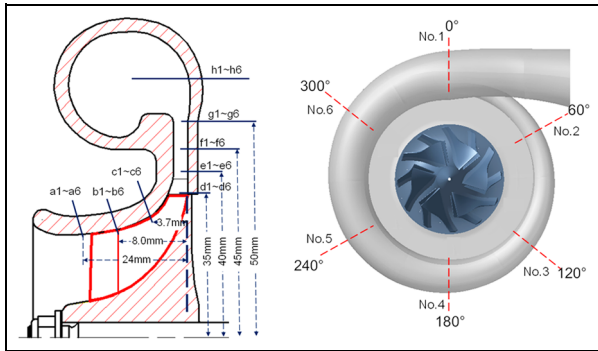
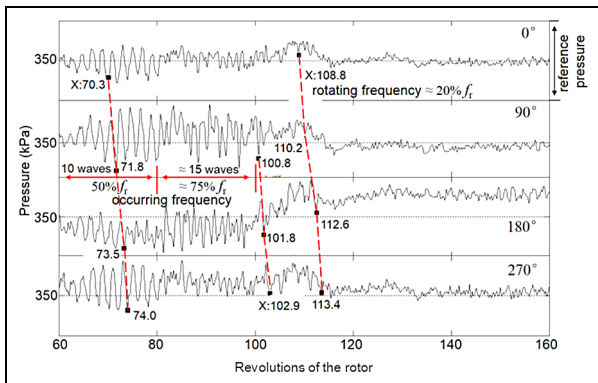**Figure 4.** Observation points for unsteady simulations.

Figure 5. Experimental results on propagation of the instability in the circumferential direction at the diffuser midsection.

circumferential direction (0° was defined at the section perpendicular to the axis of the volute exit). Point 1 at each cross-section lies at the 0° position.

Figure 5 shows the experimental results (detailed experimental information has been given by Zheng and Liu[38,39]), revealing that two types of rotating stall occurred in succession, and their frequencies were different. When looking at the period of the 60th to the 80th rotor revolutions (the time duration of this period is denoted as t_1), the number of revolutions of the rotor is 20 (the rotor frequency is $20/t_1$), whereas the pressure oscillation undergoes 10 waves (the frequency is $10/t_1$); therefore, the frequency of the rotating stall during this period is approximately 50% of the rotor frequency f_r. Similarly, the frequency of the rotating stall during the 60th to the 80th rotor revolutions is approximately 75% of the rotor frequency f_r. According to the inclined dashed line in Figure 5, when the rotor undergoes 3.7 rev (from 70.3 rev to 74.0 rev of the rotor), the signal moves from 0° to 270° (0.75 rev), allowing the calculation that the stall rotated with a circumferential speed of approximately 20% of f_r ($0.75/3.7 \approx 20\%$). Figure 6 shows the CFD results. In Figure 6(a), at the impeller midsection, the periodic stall disturbance occurred (at the positions of the cross-sections c_2 and c_3) except for the blade passing frequency, which is the main disturbance frequency. Moreover, the stall disturbance was

more obvious at the diffuser and the volute (Figure 6(b) to (d)). The frequency of the stall disturbance is approximately 75% of the rotor frequency (three waves during 4 rev of the rotors), whereas the circumferential rotational speed is approximately 22.5% of the rotor frequency. Across each monitored cross-section of the compressor, the stall disturbance is most obvious at the 60° and the 120° positions, which are numbered 2 and 3 respectively in Figure 6.

Figure 7 shows the variation in the pressure at the 120° position of each monitored cross-section. The dominant frequency at the impeller inlet is the first blade passing frequency whereas, for the other cross-sections b_3 and c_3, its first harmonic dominates. From the impeller midsection (cross-section c_3) downstream to the volute (cross-section g_3), a periodic stall disturbance occurs.

Table 3 clarifies the features of the stall obtained by the dynamic experiments and the unsteady simulations. The unsteady simulations represent the stall behaviour with great accuracy. The simulated occurring frequency and the frequency of the rotating stall in the circumferential direction were completely consistent with those of the high-frequency short-term rotating stall of the experiments. (The occurring frequency means the number of spikes obtained by a single probe during 1 s.))

Unfortunately, the unsteady simulations failed to obtain a sufficient amount of information about the low-frequency stall. Because the flow mechanism inside the compressor during the stall and surge is highly complex and because it is very difficult to obtain all the information, further investigation is necessary, and our future work will pay close attention to this topic.

Unstable flow fields

Figure 8 shows the streamline plots for different midspan sections. At the 96% span section (Figure 8(a)), the tip clearance leakage flows across the blade passage. At the 90% span section (Figure 8(b)), the streamlines at the diffuser are quite asymmetric; at the 90° circumferential position, the streamline route is short and radial (i.e. a high radial flow velocity) whereas, from 180° to 270°, the streamline route is long and tangential (i.e. a low radial flow velocity), and backflow occurs. Zheng et al.[34] showed that, for a turbocharger compressor, the asymmetric volute leads to an asymmetric flow field at the diffuser and that a low-pressure distortion exists at the 90° circumferential position downstream of the volute throttle. Thus, the low pressure at the 90° circumferential position corresponds to the high-velocity area. The flow field structures in the high-velocity areas and the low-velocity areas are quite different: in the low-velocity area, the incoming flow from the impeller inlet meets the backflow from the diffuser, which leads to 'backflow vortices' in the blade passages; in the high-velocity area, the streamlines do not travel along the
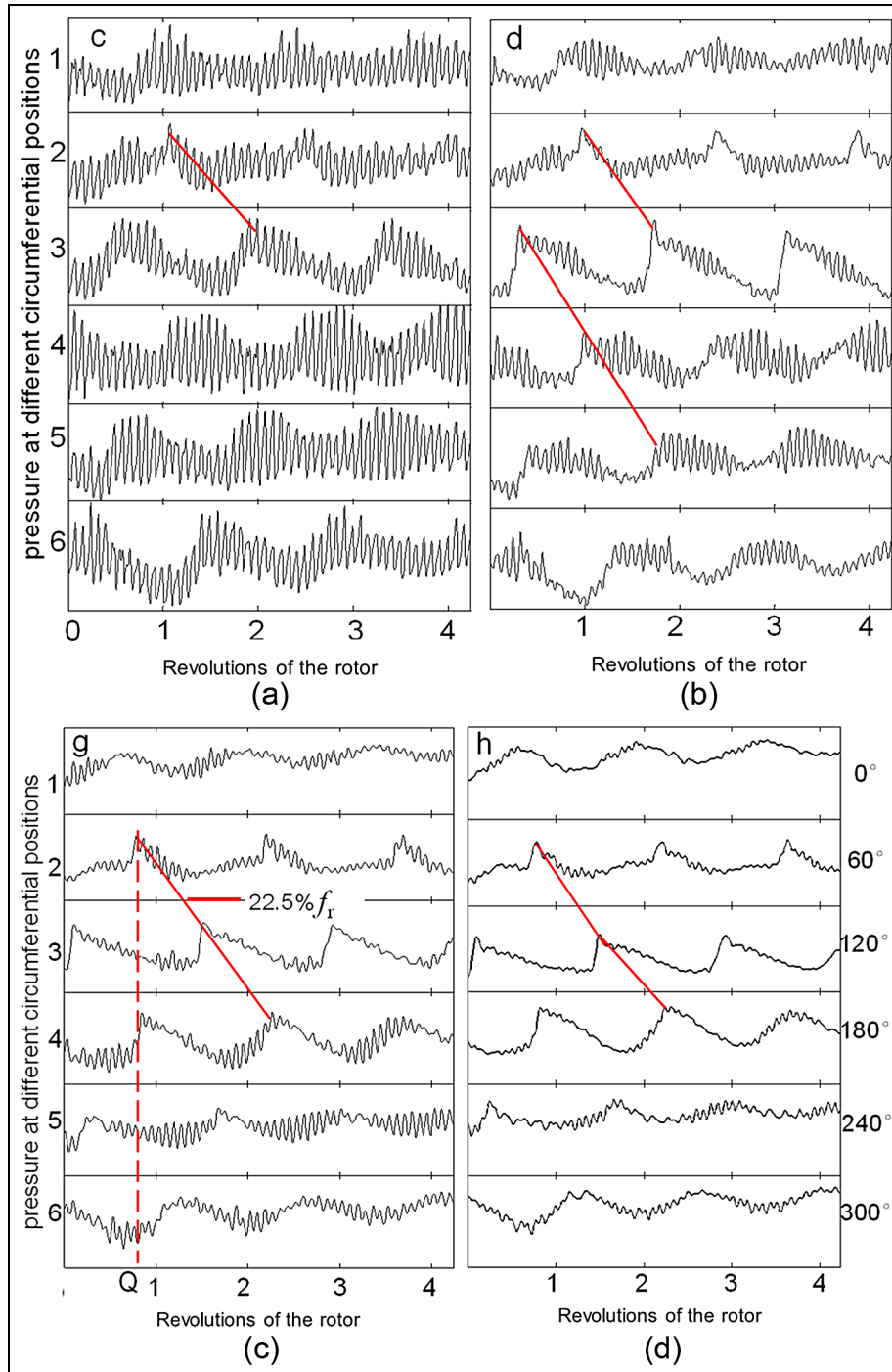
Figure 6. Variations in the pressure at different circumferential points for each cross-section from unsteady simulations: (a) cross-section *c* of the midsection of the impeller; (b) cross-section *d* of the inlet of the vaneless diffuser; (c) cross-section *g* of the outlet of the vaneless diffuser; (d) cross-section *h* of the volute.

Table 3. Stall behaviour obtained by experiments and unsteady simulations.

Deep surge in experiments Short-lived rotating stall		Unsteady simulations Rotating stall	
High-frequency (occurring)	75% f_r	Occurring frequency	75% f_r
Low-frequency (occurring)	50% f_r		
Rotational speed	20% f_r	Rotational speed	22.5% f_r
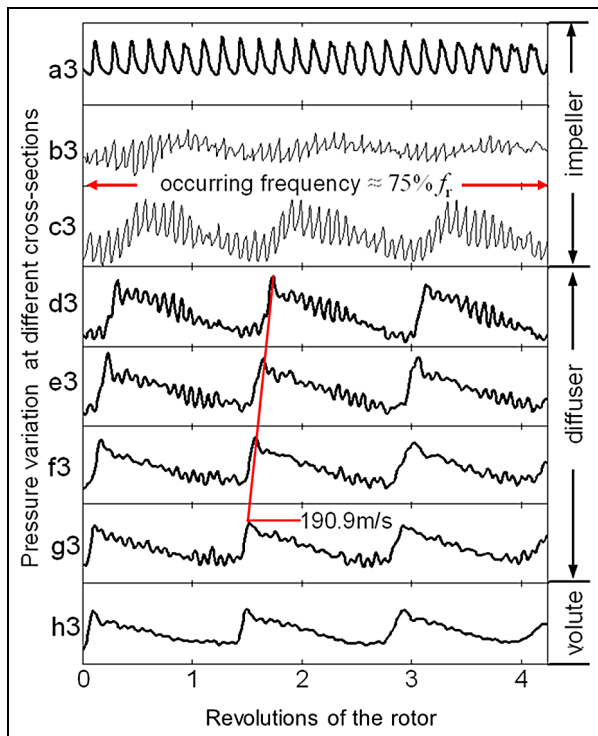
Figure 7. Variations in the pressure at different cross-sections.

Figure 8. Streamline distributions at different spans: (a) 96% span of the impeller and diffuser; (b) 90% span; (c) 70% span; (d) 50% span.

blade profile, as there is a certain amount of flow separation, but there are no large-scale backflow vortices in the blade passage. At the 70% span section, the streamlines wind along the blade profile in the high-velocity area but deviate from the blade owing to flow separation. At the 50% span section, the streamlines in all blade passages wind along the blades, and thus the instability disappears. Therefore, the unstable flow of turbocharger compressors at high rotational speeds is caused by tip clearance leakage flow, and the backflow vortices generated from interaction of the incoming flow and the backflow in the tip region of the passages.

Vo et al.[29] also proposed that the spike-type instability is caused by the tip clearance flow, the incoming flow at the leading edge and the backflow at the trailing edge from the perspective of the axial compressor. However, the backflow vortices in the blade passages and the impeller–diffuser–volute interaction were not found in their research. Below, the asymmetric flow field in the diffuser is examined to illustrate its relationship to the behaviour of the instability.

Figure 9(a) and (c) shows the averaged blade loading distributions of the main blade and the splitter blade in the high-velocity area (90°), and Figure 9(b) and (d) shows the averaged blade loading distributions of the main blade and the splitter blade in the low-velocity area (240°). In the low-velocity area, the pressure loading at the pressure side of the main blade drops at approximately 0.6–0.8 of the chord length position, which shows the occurrence of the backflow vortices; furthermore, the pressure loading at the suction side of both blades decreases towards the trailing edge,
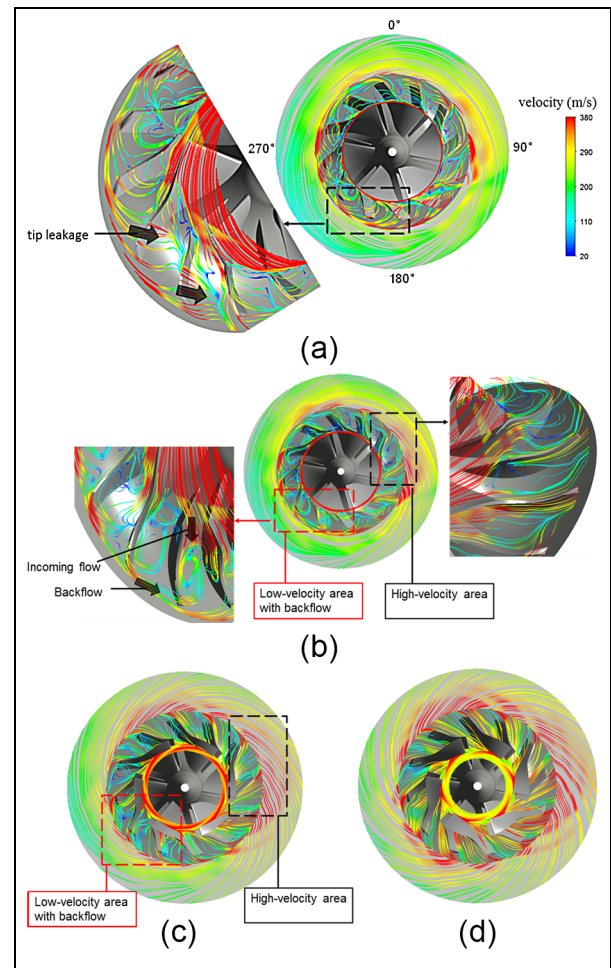
implying backflow from the diffuser. In contrast, neither of these two phenomena is reproduced in the high-velocity area (as shown in Figure 9(a) and (c)).

Figure 10 shows the pressure and the Mach number distributions in the circumferential direction at 50% blade span for different monitored cross-sections, averaged over half a rotor cycle. During the instability mode, the asymmetric volute for turbocharger compressors generates an asymmetric flow field, which is the low-pressure high-velocity area at approximately the 90° position and the high-pressure low-velocity area from approximately 180° to 270°. The high-pressure low-velocity area strengthens the backflow at the trailing edge of the impeller, which combines with the tip clearance flow to cause the backflow vortices in the corresponding impeller passages, causing a deep surge to occur. Thus, the asymmetric volute is an inducing factor for the occurrence of stall in certain impeller passages, which narrows the stable flow range of the compressor.

The flow angles at the inlet and midsection of the diffuser in the circumferential direction with different time steps are shown in Figure 11. The flow angle is defined
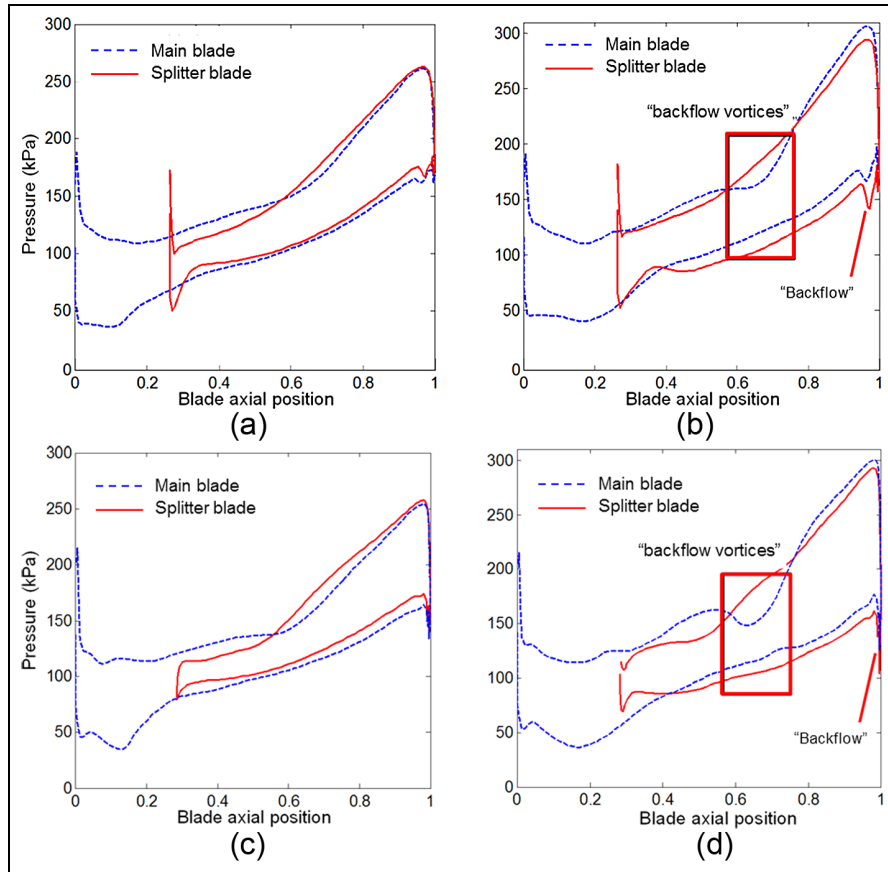
Figure 9. Averaged blade loading distributions (averaged over 1 cycle of the rotor): (a) 70% span, high-velocity area (90°); (b) 70% span, low-velocity area (240°); (c) 90% span, high-velocity area (90°); (d) 90% span, low-velocity area (240°).
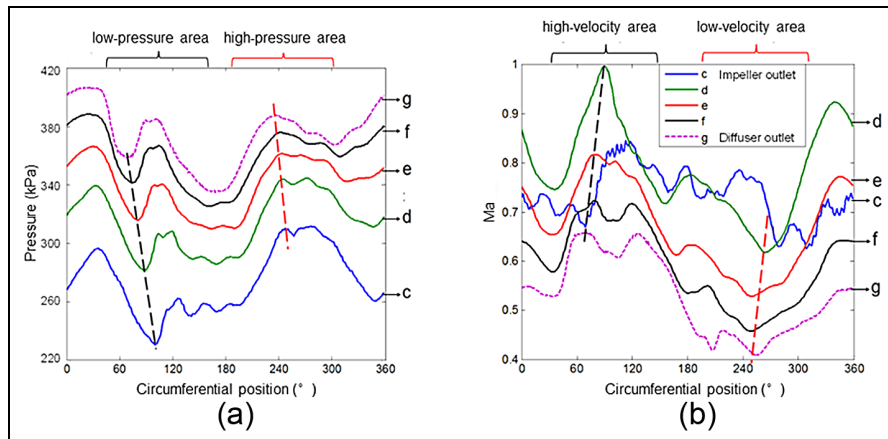

Figure 10. Averaged parameters in the circumferential direction at 50% span (averaged over 1 cycle of the rotor) of diffuser: (a) pressure; (b) Mach number.

as the flow angle between the flow and the tangential direction. The large-flow-angle region can be easily distinguished at positions from 90° to 180°, without rotation in the circumferential direction. At other positions, the flow angle is comparatively small, corresponding to the high-pressure low-velocity area in Figure 8, predicting the possibility of backflow at the impeller outlet. In addition, the occurring frequency of the rotating stall

can be judged from Figure 11, as 75% of rotor frequency f_r (approximately 3–3.5 peaks in 4.5 rev of the rotor in the large-flow-angle region).

Conclusions and remarks

In this paper, the unsteady simulation method was employed to investigate the instability in a high-speed
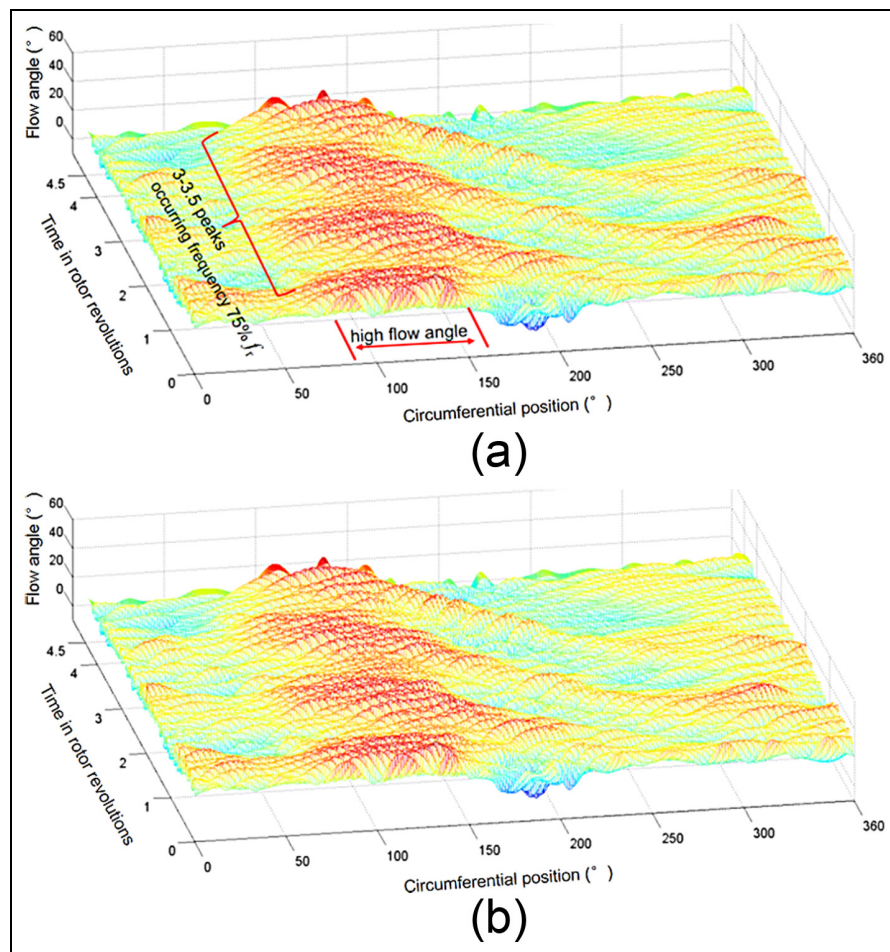
Figure 11. Flow angles in the circumferential direction at 50% span of the diffuser by unsteady simulations: (a) at the cross-section *d* of the inlet of the vaneless diffuser; (b) at the cross-section *e* of the diffuser.

turbocharger centrifugal compressor with a vaneless diffuser. Dynamic experiments based on the same compressor were used to check the accuracy of the simulation results. Some conclusions are drawn below.

1. In comparison with the experimental results, the unsteady simulations show great accuracy in representing the stall behaviour. The simulated frequency of the rotating stall is 22.5% of the rotor frequency, which agrees with that of the high-frequency short-term rotating stall obtained by experiments. The simulations also show that the stall disturbance is most obvious at the 60° and the 120° positions.
2. By investigating the flow field of the operating point of the instability, it is found that the unstable flow of turbocharger compressors at high rotational speeds is caused by the tip clearance leakage flow and the backflow vortices generated by the interaction of the incoming flow and the backflow in the tip region of the passages.
3. The asymmetric volute in turbocharger compressors generates an asymmetric flow field and, in particular, the high-pressure low-velocity area

from the 180° to the 270° circumferential positions, which strengthens the backflow at the trailing edge of the impeller. Thus, the asymmetric volute is an inducing factor for the stall behaviour in certain impeller passages. Because the volute has a significant impact on the flow field structure, it is possible to establish and develop a new volute design method which takes into account the circumferential non-uniformity of the flow field to improve the stability of the compressor; this topic needs further investigation.

Declaration of conflicting interests

Funding

References

 1. Ricardo MB, Apostolos P and Yang M. Overview of boosting options for future downsized engines. *Sci China Technol* Sci 2011; 54(2): 318–331.
 2. Clenci AC, Descombes G, Podevin P and Hara V. Some aspects concerning the combination of downsizing with turbocharging, variable compression ratio, and variable intake valve lift. *Proc IMechE Part D: J Automobile Engineering* 2007; 221(10): 1287–1294.
 3. Chiara F and Canova M. A review of energy consumption, management, and recovery in automotive systems, with considerations of future trends. *Proc IMechE Part D: J Automobile Engineering* 2013; 227(6): 914–936.
 4. Emmons HW, Pearson CF and Grant HP. Compressor surge and stall propagation. *Trans ASME* 1995; 77: 455–469.
 5. Greitzer EM. Surge and rotating stall in axial flow compressors – Part I: theoretical compression system model. *Trans ASME, J Engng Power* 1976; 98: 190–198.
 6. Greitzer EM. Surge and rotating stall in axial flow compressors – Part II: experimental results and compression. *Trans ASME, J Engng Power* 1976; 98: 199–211.
 7. Greitzer EM. The stability of pumping system – The 1980 Freeman Scholar Lecture. *Trans ASME, J Fluids Engng* 1981; 103: 193–242.
 8. Stenning AH. Rotating stall and surge. *Trans ASME, J Fluids Engng* 1980; 102: 14–20.
 9. Day IJ and Cumpsty NA. The measurement and interpretation of flow within rotating stall cells in axial compressors. *Trans ASME, J Mech Engng Sci* 1978; 20: 101–114.
10. Day IJ. *Axial compressor stall.* PhD Thesis, Cambridge University, Cambridge, UK, 1976.
11. Frigne P and Van Den Braembussche R. Distinction between different types of impeller and diffuser rotating stall in a centrifugal compressor with vaneless diffuser. *Trans ASME, J Engng Gas Turbines Power* 1984; 106: 468–474.
12. Haynes JM, Hendricks GK and Epstein AH. Active stabilization of rotating stall in a three-stage axial compressor. *Trans ASME, J Turbomach* 1994; 116: 226–239.
13. Moore FK. A theory of rotating stall of multistage axial compressors – Part I: small disturbances. *Trans ASME, J Engng Gas Turbines Power* 1984; 106: 313–320.
14. Moore FK. A theory of rotating stall of multistage axial compressors – Part II: finite disturbances. *Trans ASME, J Engng Gas Turbines Power* 1984; 106: 321–326.
15. Moore FK and Greitzer EM. A theory of post-stall transients in axial compression systems – Part I: development of equations. *Trans ASME, J Engng Gas Turbines Power* 1986; 108: 231–239.
16. Moore FK and Greitzer EM. A theory of post-stall transients in axial compression systems – Part II: application. *Trans ASME, J Eng Gas Turbines Power* 1986; 108: 231–239.
17. Bonnaure LP. *Modelling high speed multistage compressor stability.* Master's Thesis, Massachusetts Institute of Technology, Cambridge, Massachusetts, USA, 1991.
18. Spakovszky ZS and Roduner CH. Spike and modal stall inception in an advanced turbocharger centrifugal compressor. *Trans ASME, J Turbomach* 2009; 131(3): 031012.
19. Day IJ. Stall inception in axial flow compressors. *Trans ASME, J Turbomach* 1993; 115: 1–9.
20. Camp TR and Day IJ. A study of spike and stall phenomena in a low-speed axial compressor. *Trans ASME, J Turbomach* 1998; 120: 393–401.
21. Tan CS, Day I and Morris S. Spike-type compressor stall inception, detection, and control. *A Rev Fluid Mech* 2010; 42: 275–300.
22. Wernet MP, Bright MM and Shoch GJ. An investigation of surge in a high-speed centrifugal compressor using digital PIV. *Trans ASME, J Turbomach* 2001; 123: 418–428.
23. Wernet MP, Van Zante D, Strazisar TJ et al. Characterization of the tip clearance flow in an axial compressor using 3-D digital PIV. *Exp Fluids* 2005; 39: 418–428.
24. Yu XJ and Liu BJ. Stereoscopic PIV measurement of unsteady flows in an axial compressor stage. *Expl Thermal Fluid Sci* 2007; 51: 204–213.
25. Chen JP, Hathaway MD and Herrick GP. Prestall behavior of a transonic axial compressor stage via time-accurate numerical simulation. *Trans ASME, J Turbomach* 2008; 130: 041014.
26. Gourdain N, Burguburu S, Leboeuf F et al. Simulation of rotating stall in a whole stage of an axial compressor. *Comput Fluids* 2010; 39: 1644–1655.
27. Everitt JN and Spakovszky ZS. An investigation of stall inception in centrifugal compressor vaned diffuser. *Trans ASME, J. Turbomach* 2013; 135: 011025.
28. Vo HD. *Role of tip clearance flow on axial compressor stability.* PhD Thesis, Massachusetts Institute of Technology, Cambridge, Massachusetts, USA, 2001.
29. Vo HD, Tan CS and Greitzer EM. Criteria for spike initiated rotating stall. *Trans ASME, J Turbomach* 2008; 130: 011023.
30. Lei VM, Spakovszky ZS and Greitzer EM. A criterion for axial compressor hub-corner stall. *Trans ASME, J Turbomach* 2008; 130: 31006.
31. Hillewaert K and Braembussche RV. Numerical simulation of impeller volute interaction in centrifugal compressors. *Trans ASME, J Turbomach* 1999; 121: 603–608.
32. Reunanen A, Pitkanen H, Larjola J et al. Computational and experimental comparison of different volute geometries in a radial compressor. In: *ASME Turbo Expo 2000: power for land, sea, and air*, Munich, Germany, 8–11 May 2000, paper GT-469. New York: ASME.
33. Yang MY, Zheng XQ, Zhang YJ et al. Stability improvement of high-pressure-ratio turbocharger centrifugal compressor by asymmetric flow control – Part I: non-axisymmetric flow in centrifugal compressor. *Trans ASME, J Turbomach* 2013; 135:021006.
34. Zheng XQ, Huenteler J, Yang MY et al. Influence of the volute on the flow in a centrifugal compressor of a high-pressure ratio turbocharger. *Proc IMechE Part A: J Power and Energy* 2010; 224: 1157–1169.
35. Lin Y, Zheng XQ, Jin L et al. A novel experimental method to evaluate the impact of volute's asymmetry on the performance of a high pressure ratio turbocharger compressor. *Sci China Technol Sci* 2012; 55:1695−1700.
36. Zheng XQ, Jin L and Tamaki H. Influence of volute distortion on the performance of turbocharger centrifugal compressor with vane diffuser. *Sci China Technol Sci* 2013; 56: 2778–2786.
37. Zheng X, Jin L and Tamaki H. Influence of volute-induced distortion on the performance of a high-

pressure-ratio centrifugal compressor with a vaneless diffuser for turbocharger applications. *Proc IMechE Part A: J Power and Energy* 2014; 228: 440–450.

38. Zheng XQ and Liu AX. Experimental investigation of surge and stall in a high-speed centrifugal compressor. *AIAA J Propulsion Power* 2015; 31: 815–825.

39. Zheng XQ and Liu AX. Phenomenon and mechanism of two-regime-surge in a centrifugal compressor. *Trans ASME, J Turbomach* 2015; 137: 081007.

40. Hah C, Bergner J and Schiffer HP. Short length-scale rotating stall inception in a transonic axial compressor: criteria and mechanisms. In: *ASME Turbo Expo 2006: power for land, sea, and air*, Barcelona, Spain, 8–11 May 2006, paper GT2006-90045, pp. 61–70. New York: ASME.

41. Iwakiri K, Furukawa M, Ibaraki S et al. Unsteady and three-dimensional flow phenomena in a transonic centrifugal compressor impeller at rotating stall. In: *ASME Turbo Expo 2009: power for land, sea, and air*, Orlando, Florida, USA, 8–12 June 2009, paper GT2009-59516, pp. 1611–1622. New York: ASME.

42. Menter FR. Two-equation eddy-viscosity turbulence models for engineering applications. *AIAA J* 1994; 32: 1598–1605.

43. Menter FR, Langtry RB, Likki SR et al. A correlation-based transition model using local variables – Part I: model formulation. *Trans ASME, J Turbomach* 2006; 128: 413–422.